Chemisorption and thermally activated etching of Si(100)-2×1 by iodine

D. Rioux,* F. Stepniak, R. J. Pechman, and J. H. Weaver
Department of Materials Science and Chemical Engineering, University of Minnesota, Minneapolis, Minnesota 55455
(Received 19 August 1994)

Scanning tunneling microscopy (STM) and photoelectron spectroscopy were used to investigate the adsorption and thermally activated etching of Si(100)-2×1 by I_2. STM indicated that adsorption at room temperature was dissociative on Si dangling bonds without dimer disruption. Surface bonding favored occupation of both dimer atoms, but steric hindrance prevented occupation of adjacent dimers in the initial stages of adsorption. Thus, $c(4\times2)$ domains were created at ~0.5-ML coverage where alternate dimers within the same row were iodine terminated and adjacent rows were out of phase. These domains converted to a 2×1 structure when the exposure was increased. Exposure at temperatures in the range 700–900 K resulted in layer-by-layer etching with temperature-dependent morphologies and residual iodine coverages. The Si 2*p* photoemission spectra showed that Si-I bonds, Si^+, represent the dominant chemisorption structure in all cases.

INTRODUCTION

Halogen-semiconductor systems are of interest as models of surface-adsorbate interactions, and a systematic study of adsorption and etching across the halogen family reveals the influence of electronegativity and size. Molecular halogen adsorption on Si(100) is exothermic and the reactivity decreases with atomic number. For example, fluorine disrupts surface bonds and penetrates beneath the surface layer even at room temperature, whereas the less reactive, larger halogens do not.[1] Halogen adsorption on Si(100)-2×1 leads to a variety of bonding structures where chemisorption to dimer dangling bonds and adsorption at bridge sites between dimer atoms are most common.[2–10] Exposing semiconductor surfaces at elevated temperatures to a flux of halogen molecules leads to etching via the formation of volatile molecules. Such spontaneous, thermally activated processes can yield layer-by-layer etching of Si and GaAs.[11–14]

In this paper, we investigate the I_2/Si(100)-2×1 system using scanning tunneling microscopy (STM) and photoelectron spectroscopy. We demonstrate that I_2 dissociates and chemisorbs to Si dimer dangling bonds at room temperature and that steric hindrance governs the resulting structures. Analysis of STM images reveals that etching proceeds layer by layer and that the surface morphologies and amounts of residual iodine are temperature dependent. Photoemission spectra taken after etching show that SiI is the dominant halogen species, indicating that residual iodine occupies the dangling bonds. These results, in combination with data from similar experiments using Br_2 and Cl_2, reveal the influence of reactivity and size in terms of surface structure and etching.

EXPERIMENT

The experiments were performed in an ultrahigh vacuum chamber equipped with a Park Scientific Instruments STM. The base pressure of the system was $\sim5\times10^{-11}$ Torr. Silicon wafers oriented within 0.2°–0.5° of (100) and miscut toward [110] were rinsed in ethanol prior to introduction into the vacuum. The wafers were degassed at 900 K for several hours and flashed to 1475 K for 1–2 min. This procedure produces clean, well-ordered Si(100)-2×1.[15] Sample temperatures, which ranged from 700 to 900 K during exposure to I_2, were monitored with an optical pyrometer. They were accurate to within ±20 K and reproducible to ±5 K. Electrochemically etched tungsten tips were cleaned using electron bombardment. Scan dimensions were calibrated with the lattice constant of the Si(100)-2×1 surface and the height of monatomic steps. All STM micrographs were acquired in a constant current mode at room temperature using sample biases of ±0.9–2.5 V and tunneling currents of 0.2–0.5 nA. Some images show slight distortions because they were not corrected for thermal drift of the scanner.

The photoemission measurements were performed using the Minnesota-Argonne Extended Range Grasshopper/Seya monochromator and beamline at the Wisconsin Synchrotron Radiation Center. Core-level and valence-band energy distribution curves (EDC's) were collected using a double-pass cylindrical mirror analyzer in a chamber with a base pressure of $\sim5\times10^{-11}$ Torr. The overall instrumental resolutions for the Si 2*p* and I 4*d* core level spectra were ~180 and ~150 meV using photon energies of 135 and 90 eV, respectively. The EDC's were analyzed using a nonlinear least-squares minimization fitting routine.[16] Spectra were evaluated using convolved Lorentzian and Gaussian functions that represent chemically inequivalent components. The intensities and positions of these components were simultaneously optimized against a background that was represented by a cubic polynomial. Fitting parameters determined from spectra for the clean surface included the spin-orbit splitting, the branching ratio, the Lorentzian and Gaussian widths, and the energy positions of surface components.

An electrochemical cell consisting of a AgI pellet doped with CdI_2 was used to provide molecular iodine.[17] An applied voltage caused halogen ions to diffuse to a Pt

0163-1829/95/51(16)/10981(8)/$06.00

mesh electrode where they desorbed as I_2. The sample was ~3 cm from the electrode during exposures and the chamber pressure remained below 1×10^{-10} Torr during operation of the cell. Stable cell currents of 5–15 μA were used, yielding a flux of $\sim1.6\times10^{13}$ to $\sim4.8\times10^{13}$ molecules per second. Iodine exposures were done under conditions of constant flux for predetermined amounts of time. Exposures are quoted as a fluence in units of mA s. The sample was cooled rapidly to room temperature immediately upon terminating the flux. We note that the halogen flux incident on the sample depends on the experimental geometry and that sticking depends on surface conditions and temperature.

RESULTS AND DISCUSSION

A. Adsorption at 300 K

Figure 1(a) shows an occupied states image taken after exposure to 0.1 mA s at room temperature, resulting in a coverage of ~0.1 ML. Comparison to clean surface images identifies the diagonal rows as dimer rows, whereas the brighter features are iodine adsorption sites. The contrast between iodine-terminated and clean dimers could be controlled by varying the bias voltage. The dark features correspond to missing dimer (MD) defects intrinsic to the clean surface or induced by adsorption.[10] Inspection reveals two types of adsorption features (labeled *A* and *B*) that are represented schematically in Fig. 1(b). The more numerous type-*A* sites exhibit paired nodal features on the same dimer oriented parallel to the dimer bond. The paired bright features of type-*B* sites appear on adjacent dimers of the same row and occupy the same side of the row. The nodal character of type-*A* and -*B* features indicates that I_2 chemisorption is dissociative. This is consistent with molecular bond strength measurements since the Si-I bond is stronger than the I_2 molecular bond (~3.0 versus ~1.6 eV).[18] The adsorption geometry derived from the STM images and reproduced in Fig. 1(b) is consistent with halogen adsorption to Si dangling bonds without breaking dimer bonds.[10]

Pairing of adsorbates on single dimers has been noted for atomic hydrogen and bromine on Si(100)-2×1.[10,19] On clean Si(100)-2×1, the dangling bonds interact via a π bond[20] that is broken by adsorption. Therefore, adsorption of two atoms on the same dimer is favored over the adsorption of atoms on separate dimers.[21] This double occupation of dimers is preferred as long as the π bonds are stronger than the repulsive interaction between adsorbate atoms on the same dimer.[19,22,23] For iodine adsorption, the influence of the π bond is manifest in the larger population of type-*A* sites that represent doubly occupied dimers. Type-*B* sites, which have also been observed for Cl adsorption on Si(100)-2×1,[24] are less favorable because two π bonds have been removed instead of just one. Indeed, in their calculations for H adsorption on Si(100)-2×1, Vittadini, Selloni, and Casarin[21] showed that *B* sites are higher in energy than *A* sites, an effect observed here too because the number of *A* sites is much larger than the number of *B* sites. Though higher in energy, the *B* sites are derived from pairs of adsorbate atoms. For hydrogen adsorption the different pairing configuration for *B* sites is due to interactions between adjacent, singly occupied dimers.[21] Such pairing, whether as *A* or *B* features, accounts for essentially all iodine adsorption features on Si(100)-2×1.

Tip-adsorbate interactions were common after exposures less than ~0.5 mA s. While scanning with positive tip bias, iodine was often moved from one site to another or removed completely in an uncontrolled manner. The two horizontal streaks at the top of Fig. 1(a) were caused by such interactions. Type-*A* features were more susceptible to movement than *B* features. Significantly, type-*A* features move as a unit as both adatoms jump to an adjacent dimer or both are removed. The absence of single-atom events again points to the strong tendency to form pairs. Tip-adsorbate interactions decreased in frequency

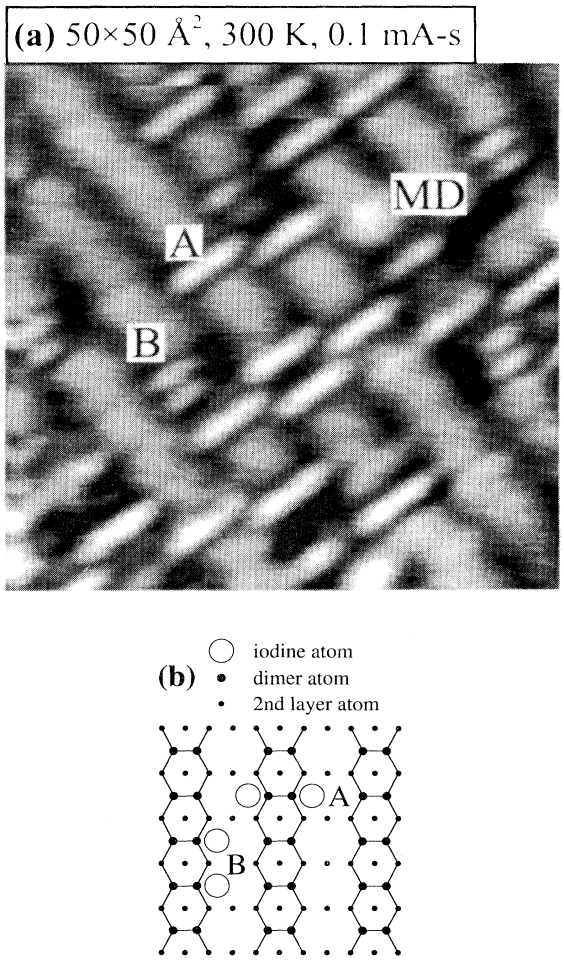

FIG. 1. (a) Occupied states image of Si(100)-2×1 showing dimer rows that run from upper left to lower right and bright features that represent iodine adsorption sites. Type-*A* sites exhibit paired nodal features on the same dimer oriented parallel to the dimer bond. Type-*B* sites are paired on adjacent dimers of the same row. Type-*A* sites are much more numerous than *B* sites. Dark areas in the image are due to missing dimer (MD) defects and other surface disruptions. (b) Schematic of type-*A* and type-*B* adsorption sites.

as the iodine coverage increased.

Figure 2(a) shows an image obtained following exposure to 0.6 mA s at room temperature, corresponding to ~0.5 ML coverage. Bright features representing *A* sites are arranged in $c(4\times2)$ domains (the dimer row direction is from lower left to upper right). Higher resolution images show iodine-terminated dimers alternating with clean dimers within the same row. Adjacent dimer rows are out of phase, as depicted in Fig. 2(b). Groups of adjacent *A* features in the same dimer row appear as longer bright segments (*S*) that are often boundaries between $c(4\times2)$ domains. Type-*B* features were rarely observed at coverages in excess of ~0.5 ML, and we conclude that they were converted to type-*A* features. Similarly, the calculations by Vittadini, Selloni, and Casarin[21] noted that type-*B* sites became less energetically favorable as the hydrogen coverage increased.

We attribute the $c(4\times2)$ structure to steric repulsion between adatoms occupying the same dimer. This forces them away from the center of the dimer and into the trough between parallel dimer rows. In turn, this prevents occupation of the dimers directly opposite in the adjacent dimer rows. The $c(4\times2)$ structure is unique to iodine among the halogens. Its absence for Br and Cl on Si(100)-2×1 reflects their smaller atomic and covalent radii.

Figure 3(a) shows that the effect of exposure to 1.1-

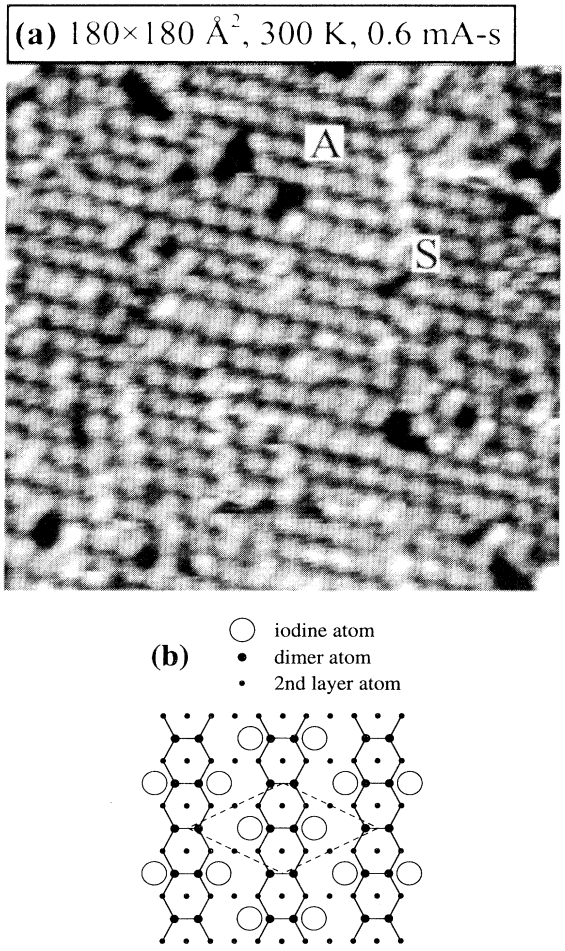

FIG. 2. (a) Occupied states image of Si(100)-2×1 showing bright features that represent individual type-*A* adsorption sites (Fig. 1) arranged in a way to create $c(4\times2)$ domains. The coverage is ~0.5 ML. Groups of adjacent type-*A* features appear as longer segments (*S*). The $c(4\times2)$ domains arise from steric repulsion between adsorbed iodine atoms. (b) Schematic showing the $c(4\times2)$ geometry created by type-*A* sites. Alternate dimers are occupied within the same row and adjacent rows are out of phase.

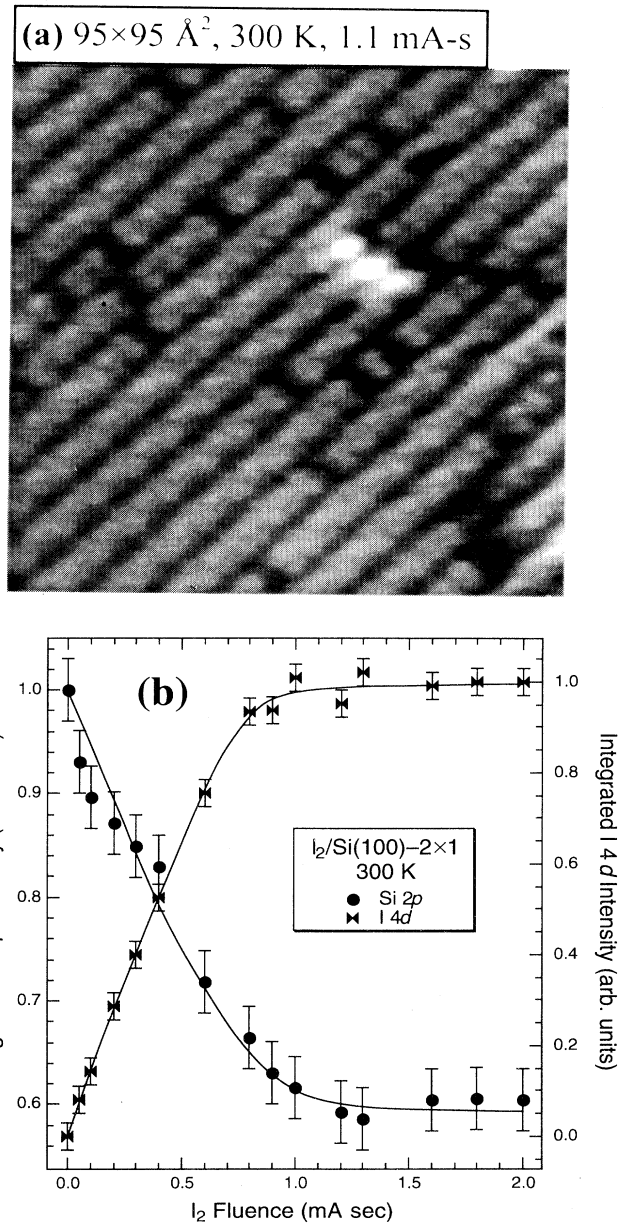

FIG. 3. (a) Occupied states image of Si(100)-2×1 after saturation exposure to I_2 at room temperature. Addition of iodine beyond 0.5 ML results in a 2×1 structure where each Si dimer is doubly occupied. Bright features represent SiI_x species that have formed but are not volatile at 300 K. (b) Normalized integrated Si 2*p* and I 4*d* core-level intensities as a function of I_2 exposure. Both curves show a flattening out at ~1.1 mA s as saturation coverage is reached.

mA s fluence is the replacement of the $c(4\times2)$ structure with a 2×1 pattern. This indicates that the iodine has filled in the holes in the low-density $c(4\times2)$ structure, resulting in the same terminal 2×1 phase as exhibited by Cl and Br. Structureless bright features in the image probably originate from SiI_x molecules created at both intrinsic and adsorption-induced defect sites. According to temperature-programmed desorption (TPD) measurements[25] these features cannot be due to adsorbed molecular iodine since I_2 desorbs at $\sim$170 K. Longer exposures yielded similar STM images, corresponding to an iodine-saturated surface.

To gain added insight into the uptake of iodine by Si(100), we recorded core-level photoemission spectra as a function of fluence. Integrated intensities of the Si $2p$ and I $4d$ core level spectra are shown in Fig. 3(b). The integrated intensity of the Si $2p$ (I $4d$) core level decreases (increases) until $\sim$1.1 mA s and then levels out. As with the STM data described above, this indicates saturation of the dimer dangling bonds. Since subsequent I_2 cannot dissociatively chemisorb, the sticking coefficient approaches zero.

Figure 4 shows representative Si $2p$ EDC's obtained before and after room-temperature exposure to I_2. The data points are presented following background subtraction, and the lines through the points correspond to the sum of chemically inequivalent components. Normalization to constant height emphasizes line-shape changes. The spectra are referenced in energy to the bulk component to compensate for changes in the surface Fermi-level position during adsorption. Surface- and bulk-sensitive spectra from the clean surface were used to determine the spin-orbit splitting (0.61 eV), the branching ratio (0.5), and the relative binding energies of chemically distinct components.

Spectrum A at the bottom of Fig. 4 was taken from the clean surface. The dominant feature corresponds to emission from bulk Si atoms while the low binding energy shoulder (S) represents surface atoms. By taking advantage of the surface sensitivity of photoelectron spectroscopy, core-level spectra can be fitted with a number of components representing different atoms in the near-surface geometry. Based on much higher resolution data than ours, Landemark *et al.*[26] associated distinct features for the clean Si(100)-2×1 core level with "up" and "down" buckled-dimer atoms, second-layer and third-layer atoms, as well as a bulk component. While we could introduce equivalent components in our fitting,[27] the data do not justify this, and the conclusion regarding the formation of Si-I bonds at the expense of dangling bonds would not be changed. Therefore, spectra B–E display only the developing Si^+ component at $\sim$0.8 eV binding energy relative to the bulk component.

Spectrum B in Fig. 4 shows the development of a chemically shifted component after I_2 exposure, corresponding to the Si^+ oxidation state. Fitting this component required a larger linewidth than the clean surface components. This accounts for the different adsorption sites, varying degrees of steric repulsion during the initial stages of adsorption, and for surface disruption at saturation. Spectra C and D show that the Si^+ component grows with exposure and that the intensity of the surface-derived component at -0.5 eV decreases until it disappears at $\sim$1 mA s. As expected, the complete attenuation of this feature in spectrum D corresponds to the saturation fluence measured in Fig. 3(b). While we made no attempt to decompose the spectra into com-

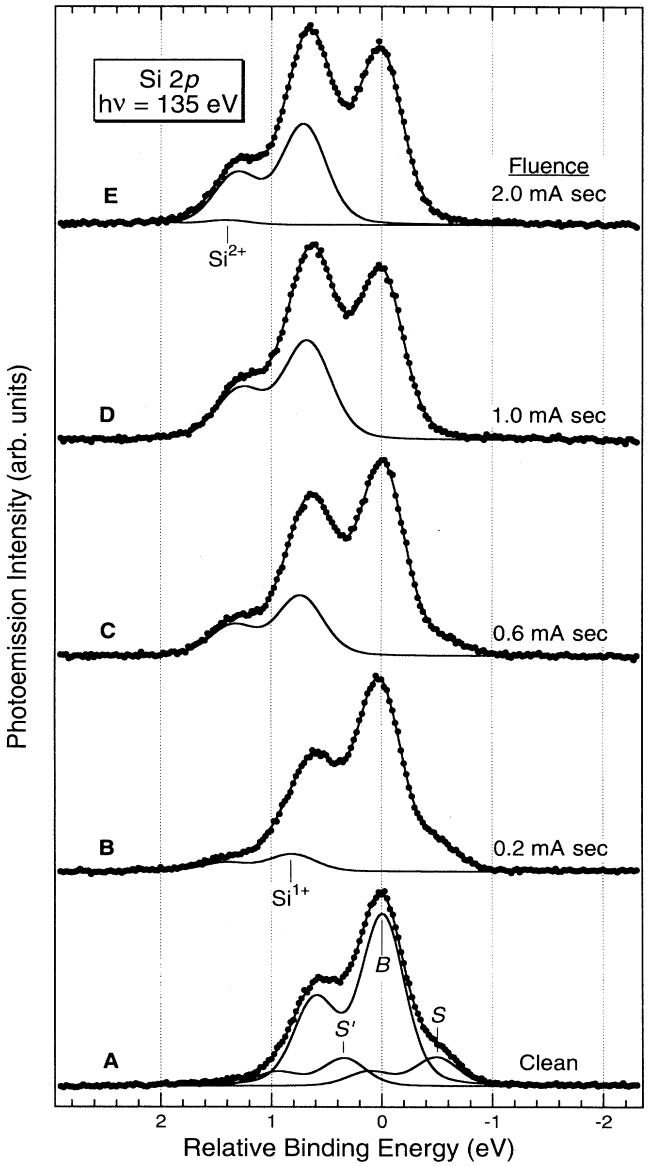

FIG. 4. Si $2p$ core-level spectra for representative I_2 exposures normalized to constant height after background subtraction. The curves drawn through the data are the sum of the fitted components (not shown). Binding energies are referenced to the bulk (B) component. The leading feature (S) of spectrum A is related to emission from the dimerized surface atoms. Component S decreases in intensity as iodine saturates the dangling bonds, and a new feature representing the Si^+ oxidation state appears. Curve D corresponds to a saturated surface, for which component S is replaced by Si^+. Further exposure results in minimal line-shape changes, but curve E has a small contribution from Si^{2+} that may reflect surface disruption and nonvolatile SiI_x.

ponents representing the A and B features of Fig. 1 or to distinguish between $c(2\times4)$ and 2×1 structures, we note that the Si^+ feature shifts from its initial relative binding energy of 0.8 eV (reflecting A and B) to 0.73 eV at saturation as measured relative to the bulk component (see Ref. 27). Finally, spectrum E shows that a small Si^{2+} component can be introduced at 1.4 eV for a fluence double the saturation coverage, but it accounts for only $\sim1\%$ of the total intensity. Clearly, SiI is the dominant surface species and what little Si^{2+} exists can be accounted for by surface disruption. The combined STM and photoemission data suggest that more iodine atoms can adsorb than are required to satisfy the dangling bonds of an ideal surface and that the extra reflects defect structures and nonvolatile reaction products.

The minimal formation of SiI_2 on Si(100)-2×1 is in contrast to what has been found for I_2 adsorption on Si(111)-7×7. In particular, Chakarian *et al.*[28] reported the formation of SiI, SiI_2, and SiI_3 in a photoemission study following room-temperature adsorption. The differences between these two systems demonstrate that Si(111) is more readily disrupted than Si(100). It will be interesting to compare the morphologies of the two surfaces using STM after exposure to halogens at elevated temperatures.

B. Etching

Surface layer etching occurred during high-temperature adsorption via the formation of volatile silicon halide products, a process that requires Si-Si bond breaking. Etching is facilitated at higher temperatures for Si(100)-2×1 because dimer bonds and back bonds are weakened. At the same time, the sticking coefficient for the impinging halogens is reduced. Accordingly, one should expect temperature dependences in the surface morphology. The images in Figs. 5–7 show representative morphologies produced by I_2 exposure at 700, 800, and 900 K, with images characteristic of the initial and advanced stages of etching.

Figure 5(a), for the initial stage of etching at 700 K, reveals pits (P) and smaller defects due to dimers that have been removed via the formation of volatile etch products. Short chains (C) on the terrace are composed of dimers that have regrown from material liberated during the etch. As for Si homoepitaxy,[29,30] these chains grow perpendicular to the terrace dimer row direction. The small-scale image in Fig. 5(b) shows that the morphology is dominated by 2×1 domains after etching a 700 K. Photoemission intensity measurements showed that both surfaces in Fig. 5 were saturated with iodine. Line-shape analysis showed that the shoulder at the leading edge of the Si $2p$ core level, representing dimer layer emission, was completely attenuated while the Si^+ component representing Si-I bonds was fully developed. Thus, we conclude that the bright oval features in Fig. 5(b) are iodine-terminated dimers while the dark features represent defects in the topmost silicon layer or missing iodine atoms.

Figure 6(a) shows that etching at 800 K produces long chains (C), large islands (I), and two-dimensional pits (P) that are elongated along the dimer row direction. Elongation indicates preferential etching that is a consequence of the disparate energies required to create S_A and S_B step edges, as observed previously for etching Si(100)-2×1 with Br.[12] Because etch products are more easily created at this higher temperature, more Si is freed so the regrowth chains and islands are larger than at

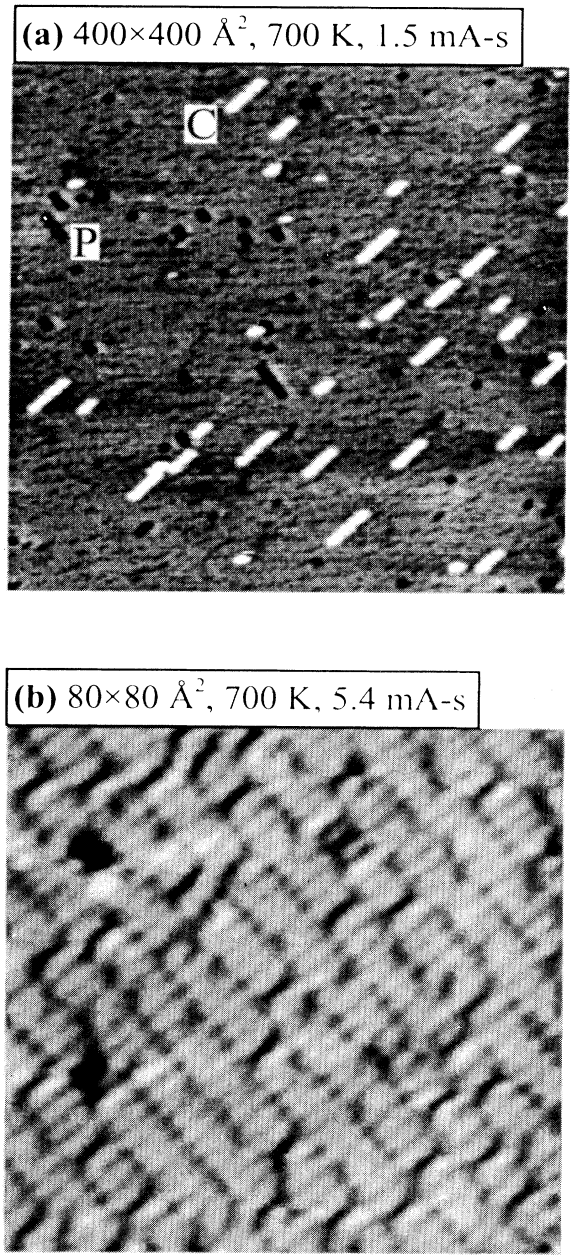

FIG. 5. Occupied states images of Si(100)-2×1 taken after etching at 700 K. (a) After the initial stage of etching, regrown dimer chains (C) appear on the terrace and single-layer pits (P) elongated along the dimer row direction are evident. (b) After short and long exposures, the surface is dominated by 2×1 domains corresponding to iodine-terminated dimers. Dimer rows run from upper left to lower right.

lower temperatures [compare to Fig. 5(a)]. For exposure at 800 K, our results show that the overall morphology does not change with longer exposure. The fact that only three layers are exposed indicates layer-by-layer removal of Si.

Figure 6(b) shows that surfaces exposed at 800 K exhibit a $c(4\times2)$ structure reminiscent of that formed after room-temperature adsorption of $\sim$0.5 ML. This arrangement of iodine is found on regrowth structures and within etch pits as well as on the terraces. Again, steric repulsion between adjacent type-*A* sites is responsible for ordering the residual adsorbate atoms. Photoemission in-

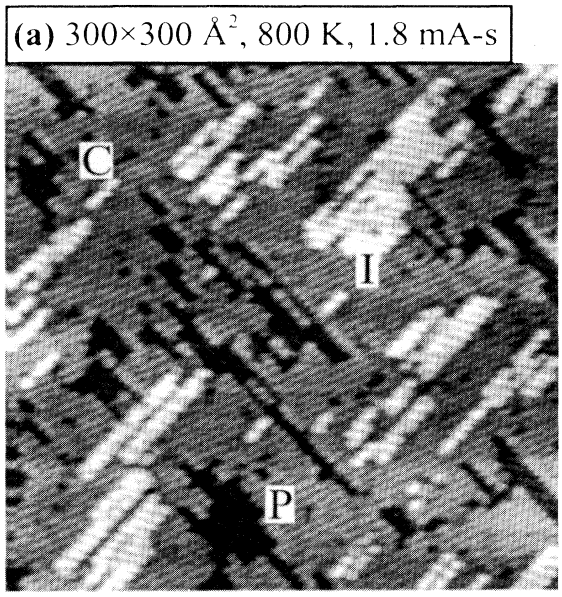

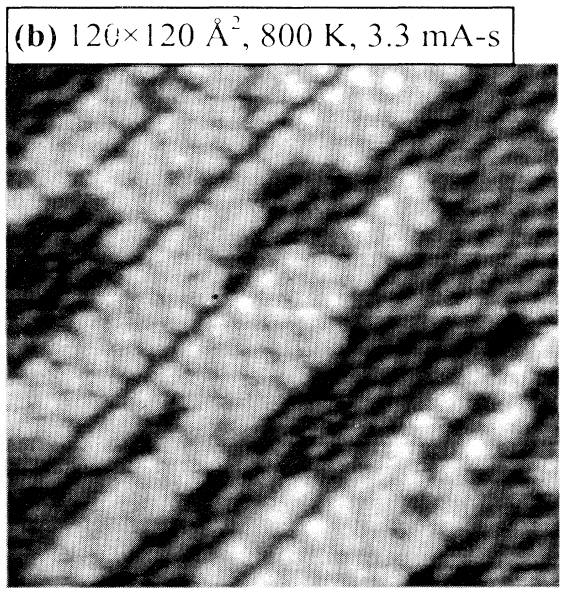

FIG. 6. Occupied states images of Si(100)-2×1 taken after etching at 800 K. (a) Surface modifications include long chains (*C*), two-dimensional islands (*I*), and pits (*P*) elongated along the dimer row direction. (b) Smaller-scale image corresponding to steady-state etching, showing little change relative to (a). A residual iodine converge of $\sim$0.5 ML results in a $c(4\times2)$ structure equivalent to that observed for room-temperature adsorption (Fig. 2). Steric repulsion mediates the ordering of the residual adsorbate atoms.

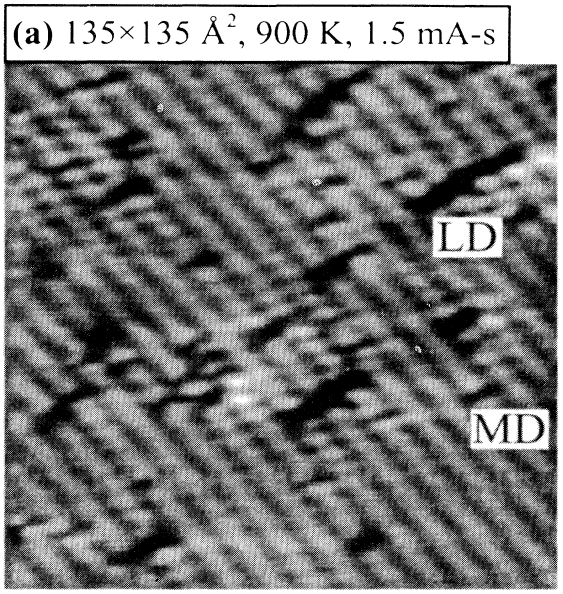

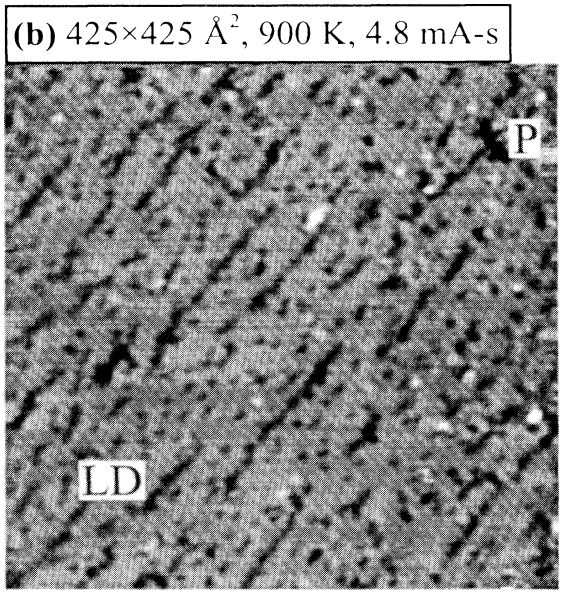

FIG. 7. Occupied states images of Si(100)-2×1 taken after etching at 900 K. (a) Very little iodine remains adsorbed and the terraces are decorated with isolated defects and small pits. The long dimension of the pits, called line defects (LD), runs perpendicular to the dimer row direction. (b) More defects are created with increasing fluence. The increase in the average line defect length indicates that the dimer vacancies interact with each other. A steady-state network of line defects with irregular pits (*P*) is ultimately achieved.

tensity measurements confirm that the coverage is ~0.5 ML when referenced to the normalized I·4*d* and Si 2*p* intensity curves for room-temperature adsorption [Fig. 3(b)]. In addition, the shoulder at the leading edge of the Si 2*p* core level recovers to approximately one-half its clean surface intensity, indicating the presence of iodine-free dimers.

Etching at 900 K results in a distinct morphology because of increased reactivity, lower residence time of I on the surface, and higher dimer vacancy mobility. Figure 7 reveals a unique etch pit structure where the pit is elongated perpendicular to the dimer rows, rather than parallel as at lower temperatures. In addition to these line defects (LD), there are many smaller pits and defects. Small-scale images reveal that very little iodine remains, a fact confirmed by photoemission intensity measurements of the I 4*d* and Si 2*p* core levels. Both observations are in agreement with TPD data that show complete desorption of adsorbed monolayers at ~900 K.[25] The Si 2*p* core level recovers the line shape of the clean surface, demonstrating that surface order is maintained to a large extent.

Following the morphology from the initial stages of etching at 900 K offers insight into LD formation. Low fluences [Fig. 7(a)] create randomly distributed MD defects and short line defects. The average defect length increases with exposure and the average spacing decreases so that the surface exhibits a network of line defects. For the steady-state surface [Fig. 7(b)] there are irregularly shaped single-layer pits (*P*) within the network. We conclude that line defect nucleation requires a minimum vacancy density and sufficient time at high temperature for diffusion processes to organize the vacancies into lines. Line defect formation has also been reported for ion-sputtered Si(100)-2×1 surfaces that were annealed between 875 and 1125 K (Refs. 31 and 32) and for surfaces etched at 1100 K using Br_2.[13] Interactions between dimer vacancies in adjacent rows are believed to cause these defects.[33]

CONCLUSIONS

Room-temperature adsorption of iodine on Si(100)-2×1 is dissociative with iodine chemisorption to dangling bonds without dimer disruption. Photoemission spectra revealed that Si-I bonds (Si^+ states) represented the dominant adsorption species. At coverages up to ~0.5 ML, iodine termination of adjacent dimers was unfavorable because of steric hindrance, and $c(4\times2)$ domains were formed where alternate dimers were free of iodine. The $c(4\times2)$ domains were converted to 2×1 by subsequent iodine uptake. Exposure at elevated temperatures resulted in single-layer etch pit formation of the terraces with arrays of line defects produced at 900 K. Terrace regrowth structures were characterized by dimer chains and two-dimensional islands. In comparison to etching using Br_2 and Cl_2 we find that the basic structures (single-layer etch pits and regrowth chains and islands) are the same but appear at different temperatures. Etching resulted in layer-by-layer removal in all cases over a wide range of temperatures.

ACKNOWLEDGMENTS

This work was supported by the Office of Naval Research. The Synchrotron Radiation Center is an NSF user facility operated by the University of Wisconsin. We thank R. Liu for assistance at the SRC and G. S. Khoo for discussion.

*Present address: Physics Department, Saint Olaf College, Northfield, MN 55057.

[1]H. F. Winters and J. W. Coburn, Surf. Sci. Rep. **14**, 161 (1992), and references therein.
[2]G. Thornton, P. L. Wincott, R. McGrath, I. T. McGovern, F. M. Quinn, D. Norman, and D. D. Vvedensky, Surf. Sci. **211/212**, 959 (1989).
[3]S. L. Bennett, C. L. Greenwood, and E. M. Williams, Surf. Sci. **290**, 267 (1993).
[4]Q. Gao, C. C. Cheng, P. J. Chen, W. J. Choyke, and J. T. Yates, Jr., J. Chem. Phys. **98**, 8308 (1993).
[5]D. Purdie, N. S. Prakash, K. G. Purcell, P. L. Wincott, and G. Thornton, Phys. Rev. B **48**, 2275 (1993).
[6]B. I. Craig and P. V. Smith, Surf. Sci. **239**, 36 (1990).
[7]T. A. Schoolcraft and B. J. Garrison, J. Vac. Sci. Technol. A **8**, 3496 (1990).
[8]C. J. Wu and E. A. Carter, Phys. Rev. B **45**, 9065 (1992).
[9]V. Eteläniemi, E. G. Michel, and G. Materlik, Surf. Sci. **251/252**, 483 (1991).
[10]D. Rioux, M. Chander, Y. Z. Li, and J. H. Weaver, Phys. Rev. B **49**, 11 071 (1994).
[11]J. S. Villarrubia and J. J. Boland, Phys. Rev. Lett. **63**, 306 (1989).
[12]M. Chander, Y. Z. Li, J. C. Patrin, and J. H. Weaver, Phys. Rev. B **47**, 13 035 (1993).
[13]D. Rioux, R. J. Pechman, M. Chander, and J. H. Weaver, Phys. Rev. B **50**, 4430 (1994).
[14]J. C. Patrin and J. H. Weaver, Phys. Rev. B **48**, 17 913 (1993).
[15]B. S. Swartzentruber, Y.-W. Mo, M. B. Webb, and M. G. Lagally, J. Vac. Sci. Technol. A **7**, 2901 (1989).
[16]J. J. Joyce, M. del Giudice, and J. H. Weaver, J. Electron Spectrosc. Relat. Phenom. **49**, 31 (1989).
[17]N. D. Spencer, P. J. Goddard, P. W. Davies, M. Kitson, and R. M. Lambert, J. Vac. Sci. Technol. A **1**, 1554 (1983).
[18]K. P. Hubert and G. Herzberg, *Molecular Spectra and Molecular Structure Constants of Diatomic Molecules* (Van Nostrand, New York, 1979).
[19]J. J. Boland, Phys. Rev. Lett. **67**, 1539 (1991).
[20]J. A. Appelbaum, G. A. Baraff, and D. R. Hamann, Phys. Rev. B **14**, 588 (1976).
[21]A. Vittatdini, A. Selloni, and M. Casarin, Phys. Rev. B **49**, 11 191 (1994).
[22]U. Höfer, L. Li, and T. F. Heinz, Phys. Rev. B **45**, 9485 (1992).
[23]M. P. D'Evelyn, Y. L. Yang, and L. F. Sutcu, J. Chem. Phys. **96**, 852 (1991).
[24]J. J. Boland, Science **262**, 1703 (1993).
[25]R. B. Jackman, R. J. Price, and J. S. Foord, Appl. Surf. Sci. **36**, 296 (1989).
[26]E. Landemark, C. J. Karlsson, Y.-C. Chao, and R. I. G. Uhrberg, Phys. Rev. Lett. **69**, 1588 (1992).

[27]The number and assignment of these shifted components to specific atoms in the near surface geometry for Si(100) has generated controversy. See Ref. 26 and also F. J. Himpsel, F. R. McFeely, A. Taleb-Ibrahimi, J. A. Yarmoff, and G. Hollinger, Phys. Rev. B **38**, 6084 (1988); G. K. Wertheim, D. M. Riffe, J. E. Rowe, and P. H. Citrin, Phys. Rev. Lett. **67**, 120 (1991); D.-S. Lin, T. Miller, and T.-C. Chiang, *ibid.* **67**, 2187 (1991); and D. H. Rich, T. Miller, and T.-C. Chiang, Phys. Rev. B **37**, 3124 (1988). It is beyond the scope of this paper to try to shed further light on this problem. For simplicity, we analyzed the data using a bulk component and two surface shifted components at -0.5 (S) and 0.35 eV (S') binding energy which attenuate with iodine exposure. The curves drawn through the data points are the sums of these components plus an evolving Si^+ component at ~ 0.8 eV relative binding energy that corresponds to Si-I bond formation.

[28]V. Chakarian, D. K. Shuh, J. A. Yarmoff, M. C. Håkansson, and U. O. Karlsson, Surf. Sci. **296**, 383 (1993).

[29]R. J. Hamers, U. K. Köhler, and J. E. Demuth, Ultramicroscopy **31**, 10 (1989).

[30]J. Y. Tsao, E. Chason, U. Koehler, and R. Hamers, Phys. Rev. B **40**, 11 951 (1989).

[31]H. Feil, H. J. W. Zandvliet, M.-H. Tsai, J. D. Dow, and I. S. T. Tsong, Phys. Rev. Lett. **69**, 3076 (1992).

[32]H. J. W. Zandvliet, H. B. Elswijk, E. J. van Loenen, and I. S. T. Tsong, Phys. Rev. B **46**, 7581 (1992).

[33]P. C. Weakliem, Z. Y. Zhang, and H. Metiu, Surf. Sci. (to be published).

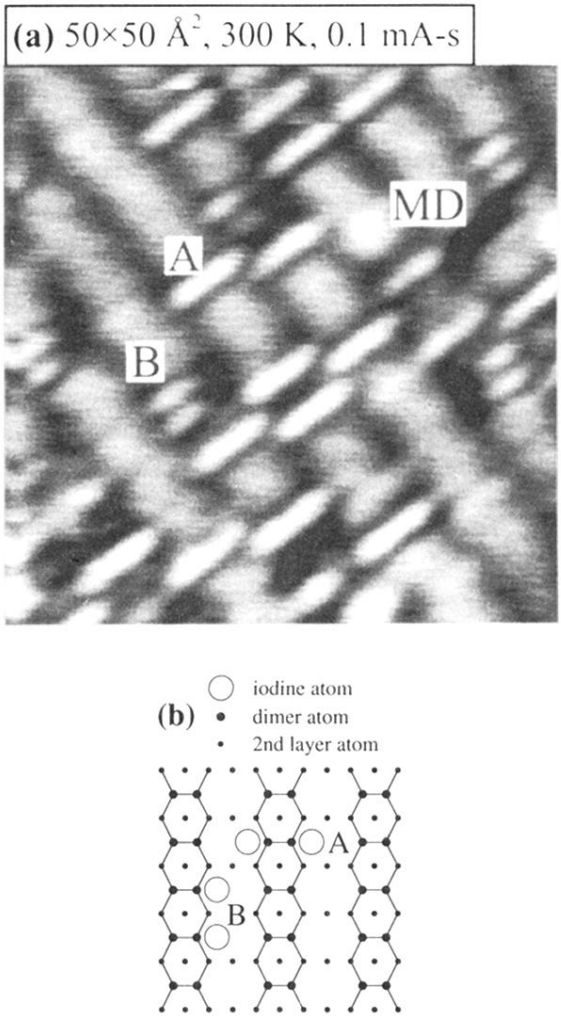

FIG. 1. (a) Occupied states image of Si(100)-2×1 showing dimer rows that run from upper left to lower right and bright features that represent iodine adsorption sites. Type-*A* sites exhibit paired nodal features on the same dimer oriented parallel to the dimer bond. Type-*B* sites are paired on adjacent dimers of the same row. Type-*A* sites are much more numerous than *B* sites. Dark areas in the image are due to missing dimer (MD) defects and other surface disruptions. (b) Schematic of type-*A* and type-*B* adsorption sites.

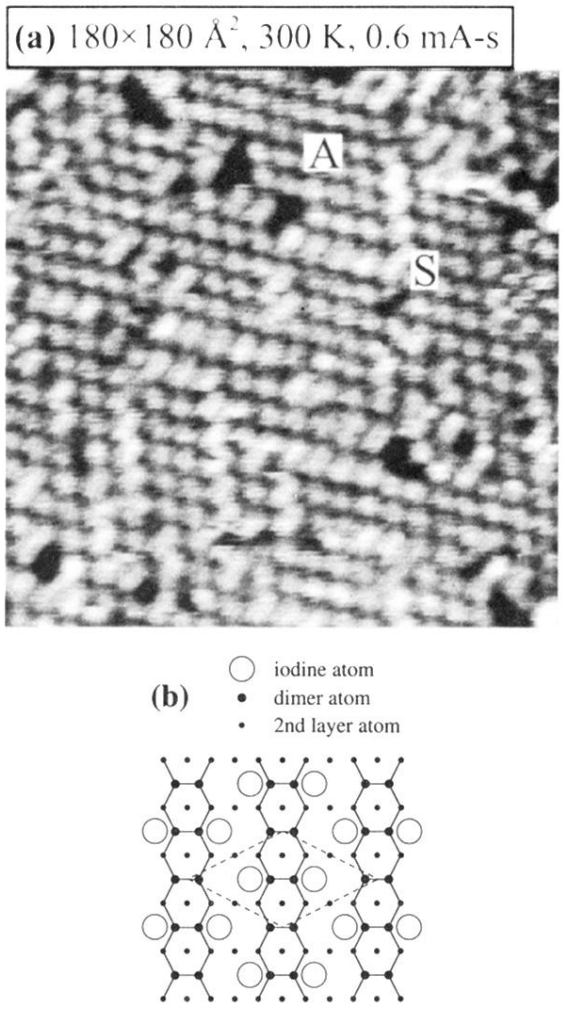

FIG. 2. (a) Occupied states image of Si(100)-2×1 showing bright features that represent individual type-*A* adsorption sites (Fig. 1) arranged in a way to create $c(4\times2)$ domains. The coverage is ~0.5 ML. Groups of adjacent type-*A* features appear as longer segments (*S*). The $c(4\times2)$ domains arise from steric repulsion between adsorbed iodine atoms. (b) Schematic showing the $c(4\times2)$ geometry created by type-*A* sites. Alternate dimers are occupied within the same row and adjacent rows are out of phase.

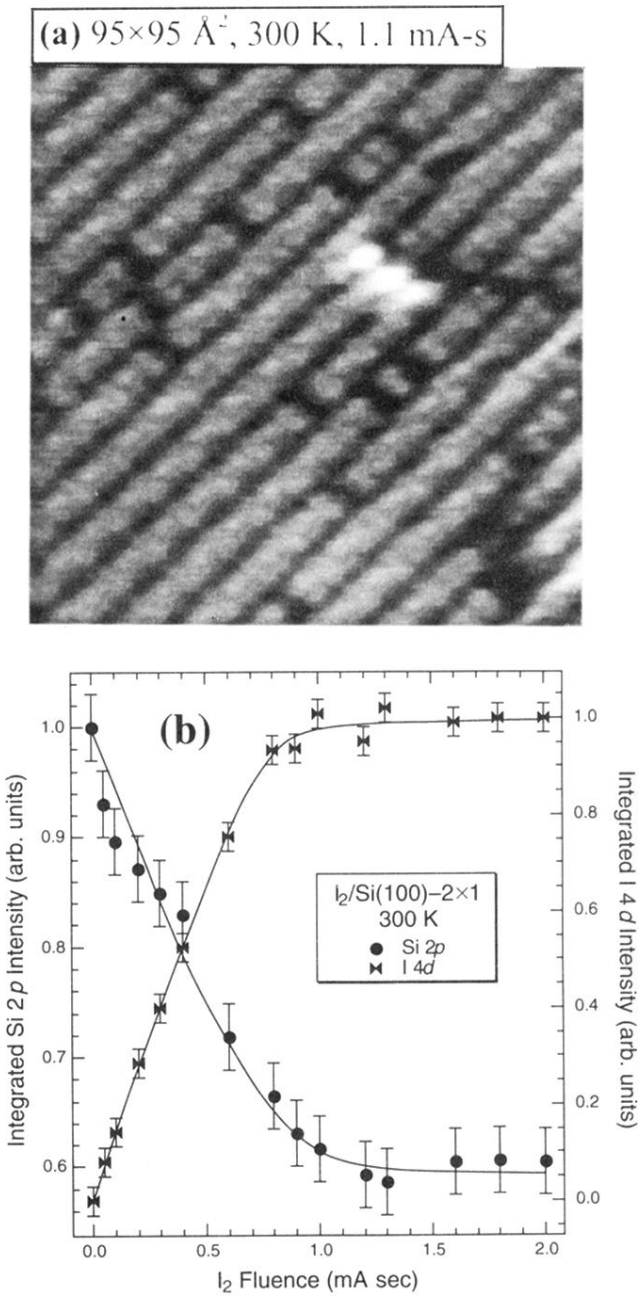

FIG. 3. (a) Occupied states image of Si(100)-2×1 after saturation exposure to I_2 at room temperature. Addition of iodine beyond 0.5 ML results in a 2×1 structure where each Si dimer is doubly occupied. Bright features represent SiI_x species that have formed but are not volatile at 300 K. (b) Normalized integrated Si 2*p* and I 4*d* core-level intensities as a function of I_2 exposure. Both curves show a flattening out at ~1.1 mA s as saturation coverage is reached.

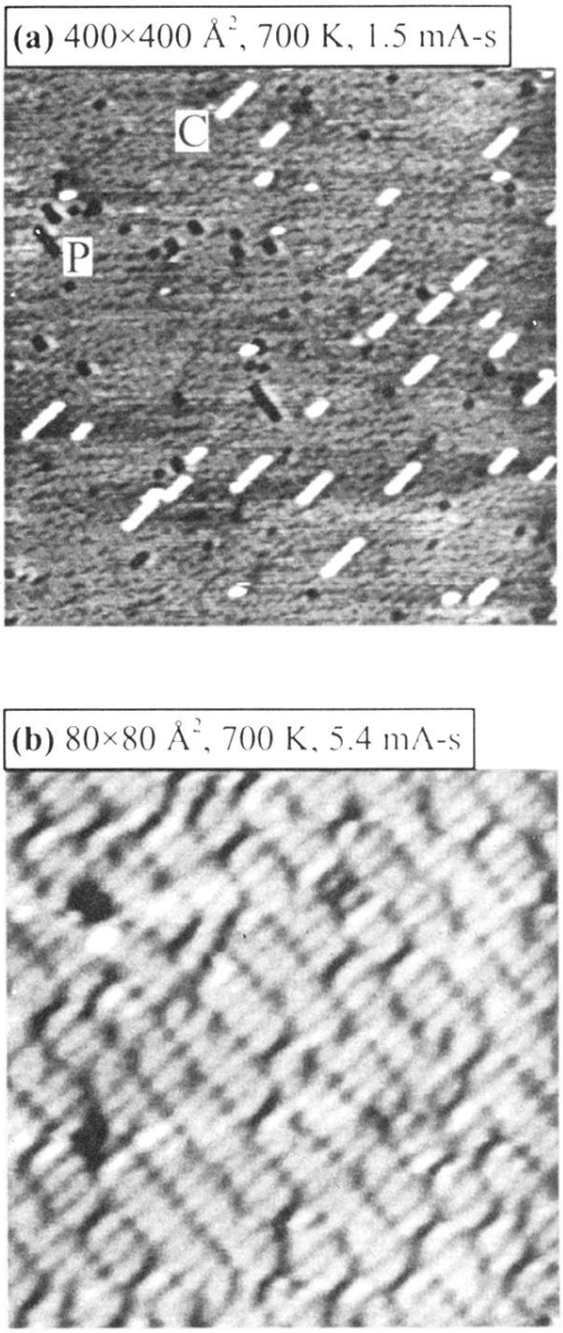

FIG. 5. Occupied states images of Si(100)-2×1 taken after etching at 700 K. (a) After the initial stage of etching, regrown dimer chains (*C*) appear on the terrace and single-layer pits (*P*) elongated along the dimer row direction are evident. (b) After short and long exposures, the surface is dominated by 2×1 domains corresponding to iodine-terminated dimers. Dimer rows run from upper left to lower right.

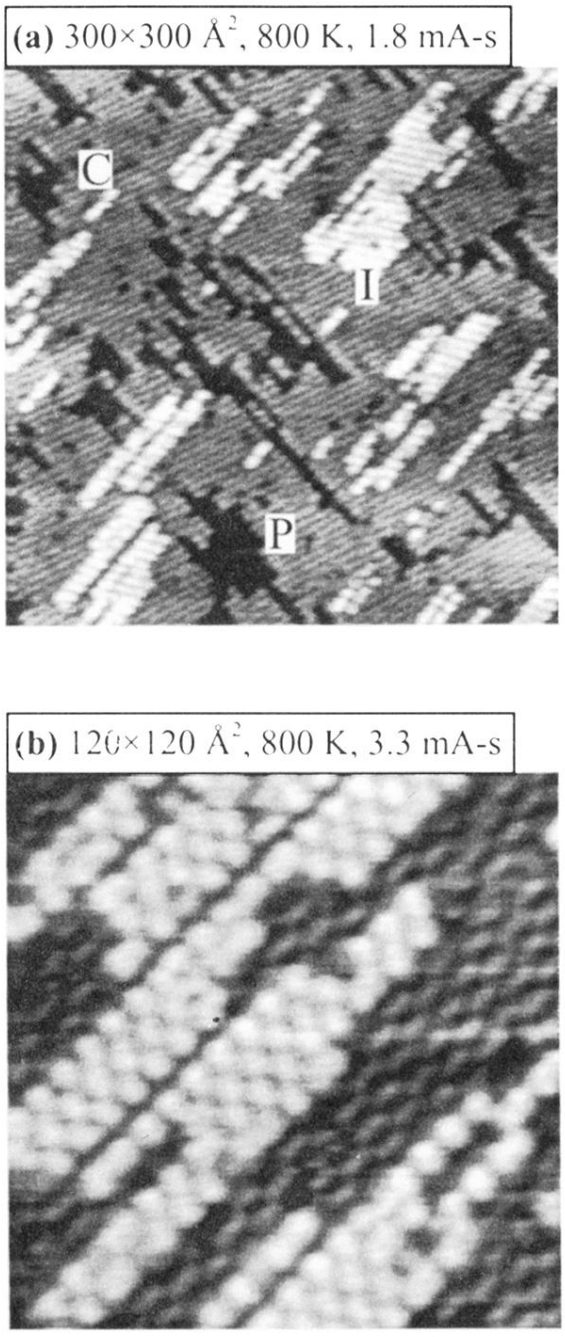

FIG. 6. Occupied states images of Si(100)-2×1 taken after etching at 800 K. (a) Surface modifications include long chains (*C*), two-dimensional islands (*I*), and pits (*P*) elongated along the dimer row direction. (b) Smaller-scale image corresponding to steady-state etching, showing little change relative to (a). A residual iodine converge of ~0.5 ML results in a $c(4\times2)$ structure equivalent to that observed for room-temperature adsorption (Fig. 2). Steric repulsion mediates the ordering of the residual adsorbate atoms.

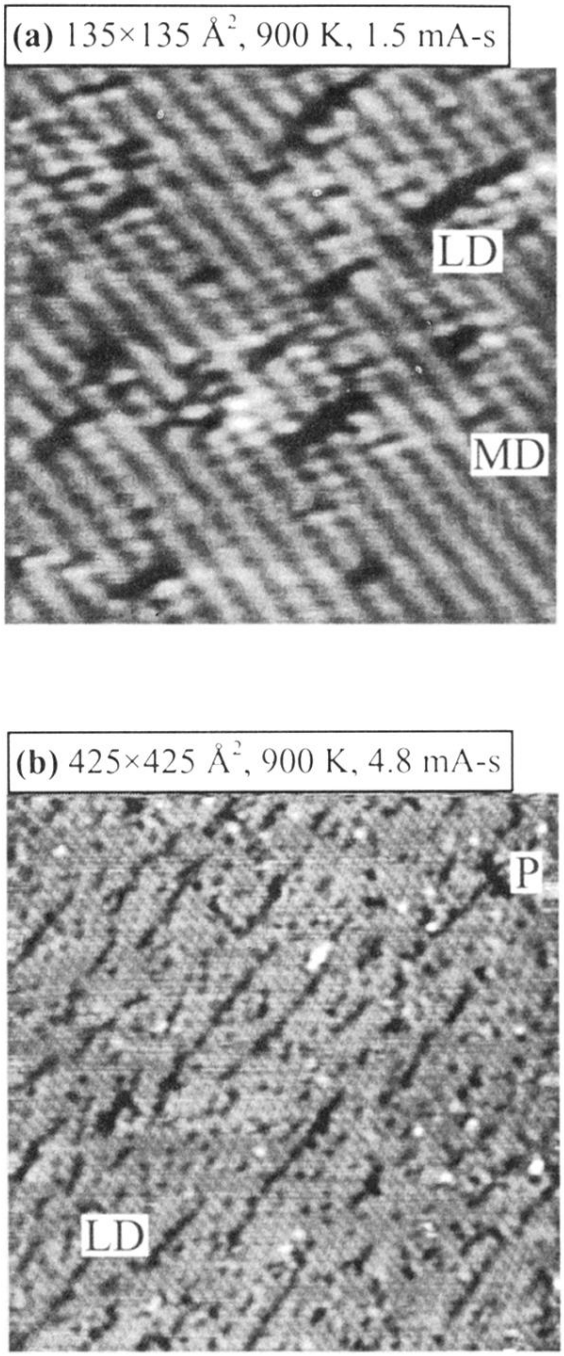

FIG. 7. Occupied states images of Si(100)-2×1 taken after etching at 900 K. (a) Very little iodine remains adsorbed and the terraces are decorated with isolated defects and small pits. The long dimension of the pits, called line defects (LD), runs perpendicular to the dimer row direction. (b) More defects are created with increasing fluence. The increase in the average line defect length indicates that the dimer vacancies interact with each other. A steady-state network of line defects with irregular pits (*P*) is ultimately achieved.